Journal of Inorganic and General Chemistry
ZAAC
Zeitschrift für anorganische und allgemeine Chemie
DOI: 10.1002/zaac.202000054
ARTICLE

Pentanucletear Nickel(II) Complex with two Vertex-Shared Triaminoguanidine Fragments and Symmetric Capping Ligand

Michael Böhme,[a][‡] Adrian E. Ion,[a][‡] Benjamin Kintzel,[a] Axel Buchholz,[a] Helmar Görls,[a] and Winfried Plass*[a]

Dedicated to Prof. Dr. Manfred Scheer on the Occasion of his 65th Birthday

Abstract. The pentanuclear nickel(II) complex $[Ni_5(saltag^{Br})_2(tptz)_4]$ (**Ni5**) with the tritopic triaminoguanidine-derived Schiff-base ligand $H_5saltag^{Br}$ (1,2,3-tris[(5-bromosalicylidene)amino]guanidine) and tptz (2,4,6-tris(2-pyridyl)-1,3,5-triazine) as capping ligands is reported. **Ni5** crystallizes in the triclinic space group $P\bar{1}$ with the central nickel(II) ion linking two triangular arrangements of nickel(II) ions supported by two tritopic triaminoguanidine ligands. The octahedral coordination of the four peripheral nickel(II) ions is complemented by capping tridentate tptz ligands. By variation of the synthesis also the corresponding trinuclear nickel(II) complex $[Ni_3(saltag^{Br})(tptz)_3]NO_3$ (**Ni3**) is accessible. Magnetic measurements for **Ni3** and **Ni5** reveal a singlet ground state with antiferromagnetic coupling between the nickel(II) ions, which in the case of **Ni5** can only be simulated assuming a two-*J* exchange coupled spin topology. For both complexes significant zero-field splitting for the nickel(II) ions is evident from the measured magnetic data, which can be verified by theoretical studies revealing a magnetic anisotropy with strong rhombic distortion due to the presence of the tptz co-ligands in both compounds.

Introduction

The design and synthesis of polynuclear transition metal complexes has received special attention over the last decades due to their relevance for topics ranging from metal active sites in biology[1] and catalysis[2] all the way to magnetism.[3] In particular, molecular magnets with a focus on single-molecule magnets (SMMs) are of interest.[4] Here, particular emphasis has been placed on ligands supporting the assembly of metal ions, especially polytopic ligands that provide multiple compartments have been used to create high-nuclear complexes with large structural variety.[5] Ligands based on triaminoguanidine are a particular class of tritopic supports for multinuclear complex arrangements.[6] Although ligands with triaminoguanidine core (see Scheme 1) have been successfully used to generate high-nuclear supramolecular assemblies with diamagnetic metal ions,[7] systems with open-shell metal ions are still rather scarce.[8] Besides two copper(II)-based coordination polymers,[9] we have reported a series of trinuclear nickel(II),[10] cobalt(II),[11] and copper(II) complexes,[12] with the latter possessing potential toward applications in molecular spintronics.[13] The most common way to connect complex fragments of different triaminoguanidine cores is either based on bridging phenolates of the tritopic ligand itself or an additional bridging ligand. However, also two cases are reported, for which a single metal ion functions as a bridging center for two triangular moieties leading to an overall pentanuclear complex fragment.[6] The latter can be viewed as competition between the coordination of a second triaminoguanidine ligand and a potential capping ligand, which can be utilized to prevent higher aggregation. For zinc(II) ions, it has been shown that this competition depends on the solvent used for reaction and crystallization.[6]

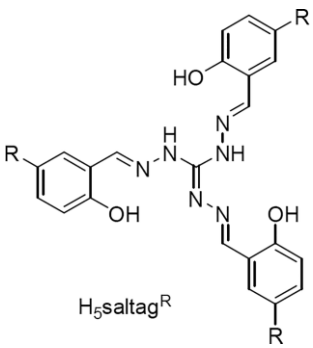

Scheme 1. Tritopic Schiff-base ligand with a triaminoguanidine core ($H_5saltag^R$).

In this context, we synthesized two polynuclear nickel(II) complexes based on the tritopic Schiff-base ligand $H_5saltag^{Br}$ {1,2,3-tris[(5-bromosalicylidene)amino]guanidine, see Scheme 1}. Depending on the reaction conditions, which include the variation of the solvent, either a trinuclear or a cor-

* Prof. Dr. W. Plass
Fax: +49 3641 948132
E-Mail: sekr.plass@uni-jena.de
[a] Institut für Anorganische und Analytische Chemie
Friedrich-Schiller-Universität Jena
Humboldtstraße 8
07743 Jena, Germany
[‡] These authors contributed equally to this article.
Supporting information for this article is available on the WWW under **http://dx.doi.org/10.1002/zaac.202000054** or from the author.

ner-shared pentanuclear complex is formed. Although such pentanuclear complexes with similar structural topology are known for several decades,[14] examples with well characterized magnetic properties are still rare and exclusively comprise complexes with high-spin ground states.[15] We particularly present and discuss the magnetic properties of the two new nickel(II) complexes, which is supported by computational studies. The challenging and so far unprecedented magnetochemistry of the pentanuclear nickel(II) system will be interpreted on the basis of the magnetic properties of the trinuclear complex in combination with high-level quantum mechanical calculations.

Results and Discussion

Syntheses

The ligand 1,2,3-tris[(5-bromosalicylidene)amino]guanidine ($H_5saltag^{Br}$) was synthesized as described in the literature via Schiff-base condensation of triaminoguanidine hydrochloride with 5-bromosalicylaldehyde and isolated as the monohydrochloride salt $H_5saltag^{Br}$·HCl.[10a,16] Subsequent addition of an aqueous solution of nickel(II) nitrate hexahydrate, a stoichiometric amount of 2,4,6-tris(2-pyridyl)-1,3,5-triazine (tptz), and aqueous tetra-*N*-butylammonium hydroxide to a solution of the ligand hydrochloride salt in methanol led to the formation of a precipitate which could be redissolved by adding *N*,*N*-dimethylformamide (dmf). The complex salt $[Ni_3(saltag^{Br})(tptz)_3]NO_3$ (**Ni3**) could be isolated as dark brown crystalline material and characterized by elemental analysis and IR spectroscopy, which is consistent with the presence of additional co-crystallized water and methanol molecules. The isolated crystals were suitable for single-crystal X-ray diffractometry.

Variation of the reaction conditions toward a less protic medium by utilizing a higher dmf portion and changing the base to triethylamine, it was possible to isolate the neutral pentanuclear nickel(II) complex $[Ni_5(saltag^{Br})_2(tptz)_4]$ (**Ni5**). Characterization of the crystalline material, which was also suitable for single-crystal X-ray diffractometry, revealed the presence of additional water and methanol molecules.

The IR spectra of both compounds show the presence of a sharp band at 1653 and 1666 cm^{-1} for **Ni3** and **Ni5**, respectively, which is characteristic for the coordinated triaminoguanidine-based ligand. In addition, an intensive band attributed to the tptz co-ligand, i.e., an aromatic CN stretching vibration, is observed in both compounds (**Ni3**: 1441 cm^{-1}; **Ni5**: 1433 cm^{-1}). The presence of the nitrate counterion in **Ni3** is confirmed by the appearance of the typical band at 1384 cm^{-1}.[17]

Structure Description

The structural data obtained for **Ni3** revealed that the complex is crystallizing in the centrosymmetric trigonal space group $R\bar{3}c$. The molecular structure obtained for the cationic complex $[Ni_3(saltag^{Br})(tptz)_3]^+$ of **Ni3** is depicted Figure 1. Due to its molecular C_3 symmetry only one crystallographically independent nickel(II) ion is present. The crystal structure contains large voids that are filled with disordered water and methanol solvent molecules. Their contribution to the structure factors was secured by back-Fourier transformation using the SQUEEZE routine of the program PLATON[18] (see Experimental Section for details).

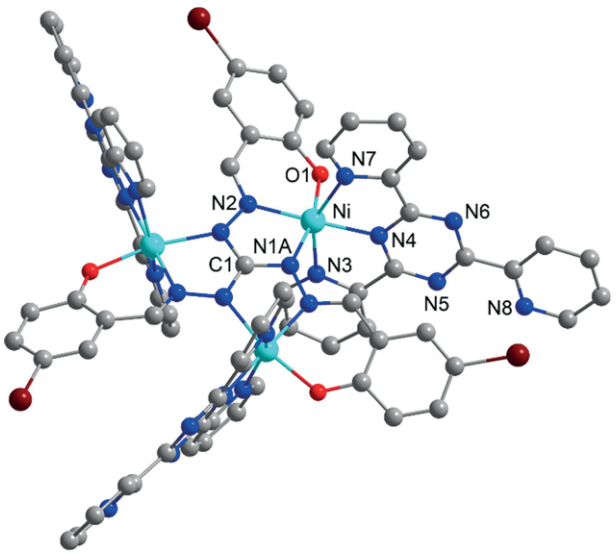

Figure 1. Molecular structure of the complex cation $[Ni_3(saltag^{Br})(tptz)_3]^+$ of **Ni3** with labels for selected atoms. Hydrogen atoms are omitted for clarity. Suffix A denotes symmetry equivalent atoms.

The central carbon atom C1 of the tritopic triaminoguanidine moiety is located on a C_3 rotational axis. The nickel(II) ion exhibits a pseudo-octahedral coordination sphere with a $[N_5O]$ donor set (for depiction of the coordination polyhedra, see Figure S1, Supporting Information), which is formed by a $[N_2O]$ coordination pocket (N1A, N2, and O1) of the tridentate deprotonated Schiff-base ligand ($H_5saltag^{Br}$) in combination with a tridentate $[N_3]$ donor set (N3, N4, and N7) provided by the tptz co-ligand. Selected bond lengths and angles for the coordination sphere of the nickel(II) ion are listed in Table S1 (Supporting Information). Continuous shape measures show a rather large deviation from an ideal octahedral coordination arrangement [$S(O_h)$ = 2.7; $S(O_h)$ = 0 refers to an ideal octahedron; see Table S2, Supporting Information] that is significantly stronger as compared to structurally similar complexes ($[Ni_3(saltag^{Br})(bpy)_3(H_2O)_3]^+$: $S(O_h)$ = 1.26; $[Ni_3(saltag^{tBu})(bpy)_3(H_2O)_3]^+$: $S(O_h)$ = 1.56).[10] The direct comparison of the pseudo-octahedral nickel(II) coordination spheres observed in **Ni3** and $[Ni_3(saltag^{Br})(bpy)_3(H_2O)_3]^+$ is visualized in Figure S2 (Supporting Information). It is evident that the distortion enforced by the rigid tptz co-ligand leads to a rather small associated *trans* angle (N3–Ni–N7 151°) as well as significantly elongated axial bond lengths [Ni–N3 218.6(4) and Ni–N7 217.9(3) pm]. As a result, the bond lengths related to the binding pocket of the tritopic bridging ligand are decreased in **Ni3** [Ni–O1: 201.3(4); Ni–N1A: 206.5(4); Ni–N2: 200.5(2) pm] compared to its 2,2′-bipyridine (bpy) analog

[Ni–O1 203.7(3), Ni–N1A 208.4(3), and Ni–N2 201.9(3) pm]. Moreover, the additional two *trans* angles associated with donor atoms of the triaminoguanidine ligand are rather close to the ideal angle of 180° [O1–Ni–N1A 166.7(1) and N2–Ni–N4 178.1(1)°].

The neutral pentanuclear complex **Ni5** crystallizes in the triclinic space group $P\bar{1}$ with two symmetry-equivalent complex molecules in the unit cell, which are related by a center of inversion. The crystal structure contains large voids that are filled with disordered water and methanol solvent molecules. Their contribution to the structure factors was secured by back-Fourier transformation using the SQUEEZE routine of the program PLATON[18] (see Experimental Section for details).

The structure of the neutral pentanuclear complex molecule **Ni5** is depicted in Figure 2 together with the illustration of the distorted pseudo-octahedral coordination polyhedra of the five nickel(II) centers (Ni0, Ni1A, Ni2A, Ni3B, and Ni4B). The suffixes A and B in the molecular structure of **Ni5** are referring to the two different tritopic Schiff-base ligands (see Figure S3, Supporting Information). Selected bond parameters for the individual nickel(II) coordination sites are given in Table S3 and the related polyhedra are visualized in Figure S4 (Supporting Information) including the corresponding donor atom labeling.

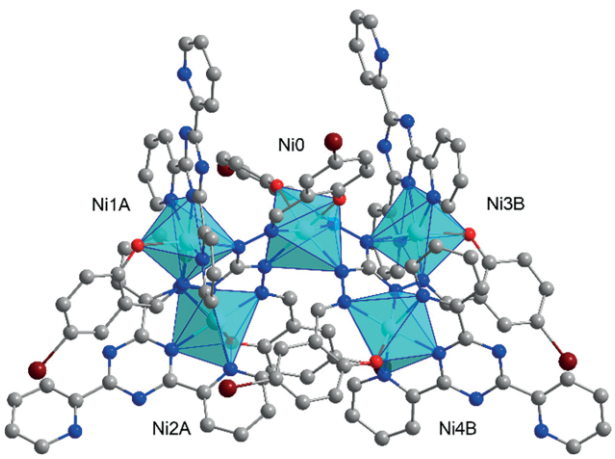

Figure 2. Structure of the neutral pentanuclear complex **Ni5** with the pseudo-octahedral coordination polyhedra of the nickel(II) ions and their labeling. Suffixes A and B denote the two different tritopic triaminoguanidine ligand moieties. Hydrogen atoms are omitted for clarity.

The central nickel(II) ion Ni0, located on a corner-shared position, is coordinated by a tridentate binding pocket of each of the two linked triaminoguanidine ligands. This leads to a distorted octahedral coordination geometry at Ni0 [$S(O_h)$ = 2.08]. On the other hand, the coordination of the tptz co-ligands at the four peripheral nickel(II) ions (Ni1A, Ni2A, Ni3B, and Ni4B) results in slightly larger distortions from the octahedral geometry [$S(O_h)$ for Ni1A/Ni2A/Ni3B/Ni4B: 2.58/2.41/2.88/2.70]. However, these distortions are still significantly smaller than those observed for the tptz-coordinated nickel(II) ions in **Ni3** (vide supra). This is due to the somewhat larger N–Ni–N *trans* angles of about 152° in the case of the peripheral nickel(II) ions of **Ni5**, as compared to 145° in **Ni3**. In addition, the axial Ni–N bond lengths of the 2-pyridyl nitrogen donors of the tptz co-ligands observed **Ni5** are significantly shorter (215–223 pm) than those found for the corresponding trinuclear complex **Ni3**.

Overall, the aforementioned structural changes between **Ni3** and **Ni5** are reflected in the slight variation of the bond lengths of the nickel(II) centers associated with the tridentate binding pockets of the tritopic saltag-based bridging ligand and the tptz co-ligand. Moreover, the virtually planar tptz co-ligands are sterically demanding and, thus, lead to an out-of-plane distortion of the π-planes of the phenolate moieties with respect to the central core of the triaminoguanidine ligands in complex **Ni3** with a dihedral angle of 22° (see Figure S5, Supporting Information). A similar distortion is found for **Ni5** with dihedral angles in the range 19° to 26° for the peripheral nickel(II) centers (Ni1A 22.1°, Ni2A 22.1°, Ni3B 25.9°, and Ni4B 19.4°), whereas for the phenolate moieties at the bridging nickel(II) center Ni0 dihedral angles of 12.5° (ligand A) and 40.7° (ligand B) are observed.

Magnetic Measurements

The magnetochemistry of **Ni3** and **Ni5** was studied by temperature dependent dc magnetic susceptibility measurements in the temperature range between 2 and 300 K. For structural reasons, a one-*J* and a two-*J* spin topology can be assigned for **Ni3** and **Ni5**, respectively, as depicted in Scheme 2. This is strictly given by symmetry for **Ni3**, while for **Ni5** it is based on structural characteristics of the relevant nickel(II) centers in the molecular structure, which can be divided in two groups, the peripheral nickel(II) ions (Ni1A, Ni2A, Ni3B, and Ni4B) and the central bridging nickel(II) ion (Ni0).

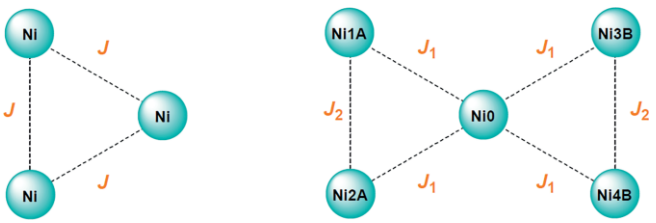

Scheme 2. Spin topologies of the exchange coupling schemes of **Ni3** (left) and **Ni5** (right).

Trinuclear Complex Ni3

The temperature dependent magnetic susceptibility data $\chi_M T$ and magnetization data M for **Ni3** are depicted in Figure 3. The room temperature $\chi_M T$ value is 2.80 $cm^3 \cdot K \cdot mol^{-1}$, which is slightly lower than the related spin-only value (3.0 $cm^3 \cdot K \cdot mol^{-1}$, g = 2), indicating antiferromagnetic exchange interactions. This is consistent with the decrease of $\chi_M T$ upon lowering the temperature to a value of 0.06 $cm^3 \cdot K \cdot mol^{-1}$ at 2 K, which confirms the presence of a diamagnetic ground state (S = 0). It should be noted that such a diamagnetic ground state is well documented for triangular nickel(II) complexes with C_3 symmetry and antiferromagnetic exchange interaction.[10] The reduced magnetization data

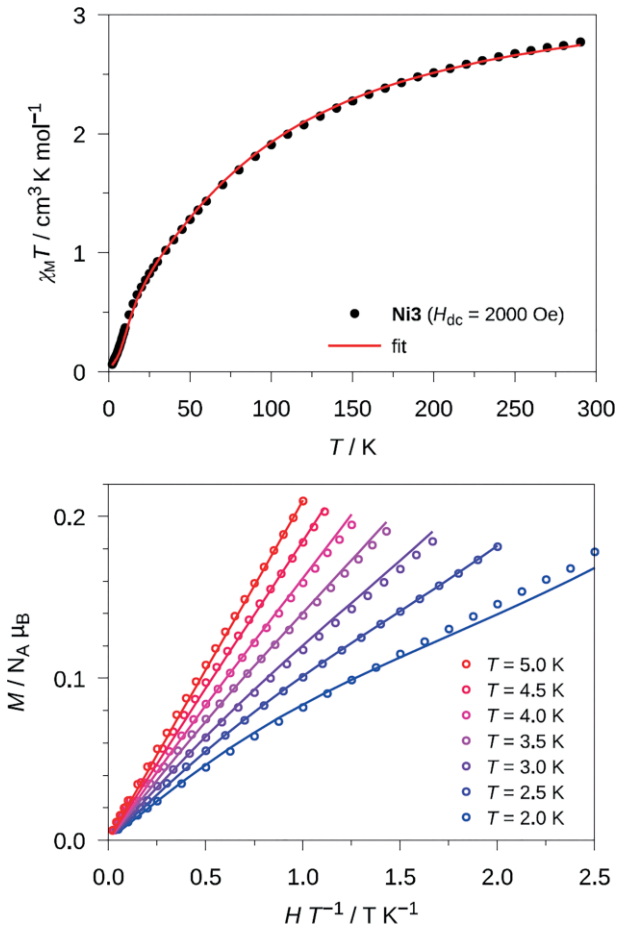

Figure 3. Top: Temperature dependence of $\chi_M T$ for the trinuclear nickel(II) complex **Ni3** depicted as black dots (●). Bottom: Variable-field magnetization data $M(H/T)$ for **Ni3** at different temperatures depicted as circles (○). The solid colored lines represent the best simultaneous fit of magnetic susceptibility and magnetization data including a zero-field splitting contribution (see text).

$M(H/T)$ for **Ni3** presented in Figure 3 indicates the presence of magnetic anisotropy. To extract magnetic parameters from experimental data, the temperature dependent $\chi_M T$ values as well as the magnetization data of **Ni3** were fitted simultaneously with the Hamiltonian given in Equation (1) (see Scheme 2) using the program PHI.[19]

$$\hat{H} = -J(\hat{S}_1\hat{S}_2 + \hat{S}_2\hat{S}_3 + \hat{S}_1\hat{S}_3) + D\sum_{i=1}^{3}[\hat{S}_{z,i}^2 - \tfrac{1}{3}S(S+1)] + g\mu_B\vec{H}\sum_{i=1}^{3}\hat{S}_i \quad (1)$$

Besides the exchange coupling constant J, the Hamiltonian includes an axial zero-field splitting (ZFS) parameter D, which is identical for all nickel(II) ions due to the C_3 symmetry of the complex cation in **Ni3**. The data were corrected for a small paramagnetic impurity indicated by the non-zero $\chi_M T$ value at 2 K (ρ = 3.9%). The best fit for the magnetic data of **Ni3** results in an antiferromagnetic coupling constant J = –29.1 cm^{-1} with an isotropic g value of 2.138, which is in good agreement with the values reported for similar trinuclear nickel(II) complexes.[10] The axial ZFS parameter was found to be essential for the fitting of the data and converged to a value of D = 20.4 cm^{-1}. The positive sign of D indicates a magnetic anisotropy of easy-plane type. The presence of magnetic anisotropy was also confirmed by solely fitting the magnetic susceptibility data (denoted as Fit II in Table S4; see also Figure S6, Supporting Information). Although this leads to an underestimation of the axial ZFS parameter, the exchange coupling constant obtained by both fits is only slightly changed (cf. Table S4).

In this context, it is interesting to note that for the similar compound $[Ni_3(saltag^{tBu})(bpy)_3(H_2O)_3]Cl$ an axial ZFS parameter D could not be obtained directly by fitting the magnetic susceptibility data.[10b] Therefore, we conclude that based on the presence of the tptz co-ligand in **Ni3** the stronger distortion of the nickel(II) pseudo-octahedral coordination spheres leads to a significantly larger ZFS than in the previous case with bpy co-ligand (vide supra).

*Pentanuclear Complex **Ni5***

In Figure 4 the temperature dependent $\chi_M T$ data for the pentanuclear complex **Ni5** is depicted. As in the case of **Ni3** the room temperature $\chi_M T$ value of 4.67 cm^3·K·mol^{-1} is some-

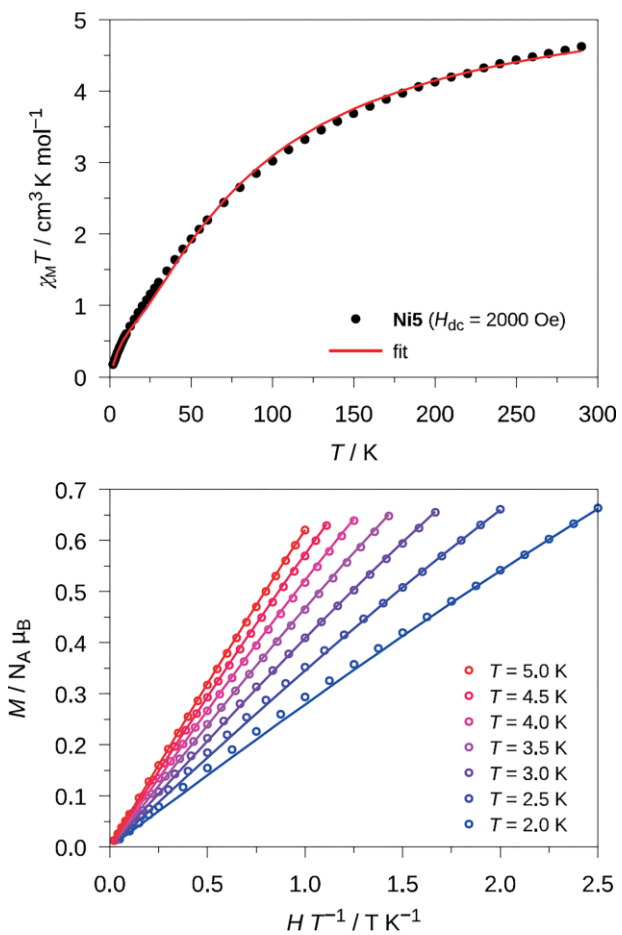

Figure 4. Top: Temperature dependence of $\chi_M T$ for the pentanuclear nickel(II) complex **Ni5** depicted as black dots (●). Bottom: Variable-field magnetization data $M(H/T)$ for **Ni5** at different temperatures depicted as circles (○). The solid colored lines represent the best simultaneous fit of magnetic susceptibility and magnetization data including a zero-field splitting contribution (see text).

what smaller than the expected spin-only value for an uncoupled pentanuclear system (5.0 cm^3·K·mol^{-1}, g = 2.0). Together with the observed decrease in the $\chi_M T$ values with decreasing temperature, this clearly indicates the presence of antiferromagnetic exchange interactions within the pentanuclear spin system. At 2 K a $\chi_M T$ value of 0.18 cm^3·K·mol^{-1} is reached. Consistent with magnetization measurements this leads to the assignment of a diamagnetic ground state (S = 0), which to the best of our knowledge is in contrast to all other pentanuclear nickel(II) complexes with a comparable spin topology showing high-spin ground states (S = 3).[15]

The spin topology in **Ni5** is graphically represented in Scheme 2 and can be described as a "butterfly" motif formed by two corner-shared triangular units, which are linked by the central nickel(II) ion Ni0. This spin topology assumes two different types of magnetic interactions (Scheme 2): (i) Exchange coupling constant J_1 between the central ion (Ni0) and the peripheral ions (Ni1A, Ni2A, Ni3B, and Ni4B). (ii) Exchange coupling constant for the interaction between the two pairs of peripheral ions (Ni1A/Ni2A and Ni3B/Ni4B) denoted as J_2. This is a justified simplification of the spin topology, although the structure of **Ni5** contains five crystallographically independent nickel(II) ions, since the main exchange path is expected to be through the core of the bridging triaminoguanidine ligands. Moreover, the overall number of parameters has to be kept at a minimum to avoid overparameterization with possible correlations between parameters during the fit procedure. The corresponding spin Hamiltonian for **Ni5** is given in Equation (2):

$$\hat{H} = -J_1(\hat{S}_0\hat{S}_1 + \hat{S}_0\hat{S}_2 + \hat{S}_0\hat{S}_3 + \hat{S}_0\hat{S}_4) - J_2(\hat{S}_1\hat{S}_2 + \hat{S}_3\hat{S}_4) + \sum_{i=0}^{4} D_i[\hat{S}_{z,i}^2 - \tfrac{1}{3}S(S+1)] + g\mu_B\vec{H}\sum_{i=0}^{4}\hat{S}_i \quad (2)$$

As in the case of **Ni3**, the Hamiltonian in addition to the exchange interactions includes axial ZFS parameters D for the individual nickel(II) ions. Although a slight difference between the central and the peripheral nickel(II) ions can be expected from structural data, which is confirmed by ab initio multireference calculations (vide infra), for numerical simulations of the experimental data all D parameters need to be assumed as identical to essentially avoid overparameterization.

Before starting with the analysis of the magnetic data, it is worth to first shed some light on the situation resulting from the competing exchange interactions[20] in **Ni5** (Scheme 2), which is due to the presence of antiferromagnetic coupling between the nickel(II) ions. The given spin topology leads to a rather complicated energy spectrum of spin states, which depends on the ratio J_2/J_1 of the two exchange coupling constants. The corresponding energy level scheme neglecting ZFS contributions for the individual nickel(II) ions is depicted in Figure 5. It is apparent that for the case of $J_1 = J_2$ this leads to a situation for the ground state in which a diamagnetic singlet (S = 0; $J_2 < J_1 < 0$) and a triplet state (S = 1; $J_1 < J_2 < 0$) are degenerate. Moreover, for cases slightly deviating from this situation the energy splitting between these two states ΔE directly correlates with the difference in the coupling constants J_1 and J_2 ($\Delta E = |J_1 - J_2|$). In addition, for ratios $J_2/J_1 < 0.5$ and $J_2/J_1 > 2.0$ the magnetic spin ground state is expected to be S = 3 and S = 1, respectively. Unfortunately, the situation gets more complicated if magnetic anisotropy is taken into account, which results in a further splitting of the degenerate (2S+1)-fold spin multiplets with $S > 0$ and formally can affect the spin ground state. Based on these considerations, various approaches were taken into account to simulate the experimental magnetic susceptibility data of **Ni5**.

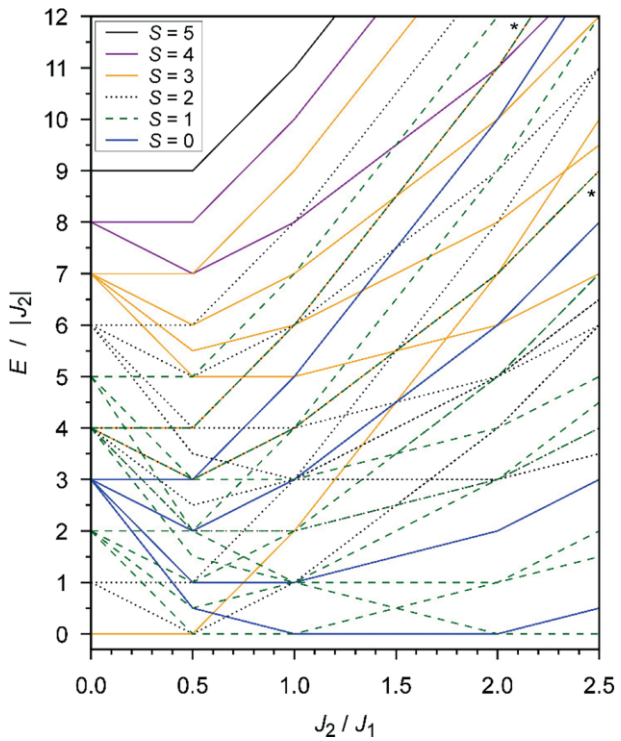

Figure 5. Variation of the spin state energies for the spin topology of two corner-shared isosceles triangles as observed in **Ni5** with all local spins of S = 1 (neglecting ZFS contributions) vs. the ratio J_2/J_1 (see Scheme 2 and text) with the energy of the ground state taken as energy origin; J_1 and J_2 are assumed to be negative; for the lines marked with an asterisk three spin states (S = 1, 2, and 3) are lying on top of each other.

To obtain initial parameters for further magnetic fits, at first only the magnetic susceptibility data of **Ni5** measured in the temperature range between 2 to 300 K was fitted utilizing the Hamiltonian given in Equation (2), however, employing an identical axial ZFS parameter D for all five paramagnetic nickel(II) centers (denoted Fit I in Figure S7 and Table S5, Supporting Information) to avoid overparameterization. This results in two rather similar magnetic coupling constants of J_1 = –31.4 cm^{-1} and J_2 = –38.1 cm^{-1} consistent with the overall antiferromagnetic exchange in **Ni5**. The obtained ratio J_2/J_1 of 1.21 determines a S = 0 magnetic ground state in **Ni5** (see Figure 5). The magnetic exchange between the terminal ions Ni1A···Ni2A as well as Ni3B···Ni4B (see Scheme 2) as represented by J_2, despite the structural similarity, seems to be stronger than the corresponding one obtained for **Ni3** (–29.1 cm^{-1}). The isotropic g value of 2.193 is only slightly larger than the value observed for **Ni3**, whereas the absolute value of the average ZFS parameter for the five nickel(II) cen-

ters from this fit ($|D| = 40.0\ cm^{-1}$) is considerably larger than the ZFS observed for **Ni3** ($D = 20.4\ cm^{-1}$).

In order to investigate the effect of enforcing an identical axial ZFS parameter for all five nickel(II) ions, a second approach denoted as Fit II was employed for the simulation of the experimental magnetic susceptibility data. In this approach, the ZFS parameters were still fixed, but to the individual values obtained from ab initio multi-reference calculations (vide infra; **Ni0/Ni1A/Ni2A/Ni3B/Ni4B**: –10.7/–13.9/–13.5/–14.9/14.4 cm^{-1}). Although rather similar magnetic parameters were obtained, this simulation results in somewhat more differentiated magnetic coupling constants $J_1 = –20.8\ cm^{-1}$ and $J_2 = –33.3\ cm^{-1}$ ($g = 2.121$, cf. Table S5, Supporting Information) than found for Fit I. The ratio J_2/J_1 of 1.60 is consistent with a $S = 0$ magnetic ground state. Moreover, this simulation approach resulted in a J_2 parameter of $–33.3\ cm^{-1}$ which is more consistent with the one obtained for **Ni3** ($–29.1\ cm^{-1}$) as compared to the J_2 value obtained for **Ni5** in Fit I ($–38.1\ cm^{-1}$).

In a third approach the magnetic susceptibility data and magnetization data of **Ni5** were used for simultaneous fit based on Equation (2) (see Figure 4; denoted as Fit III in Table S5, Supporting Information). For this approach, the magnetic parameters obtained by Fit II in combination with the axial ZFS parameter D obtained for **Ni3** were used as initial starting parameters. The obtained best-fit parameters are $J_1 = –20.8\ cm^{-1}$, $J_2 = –37.3\ cm^{-1}$, $D = 16.6\ cm^{-1}$, and $g = 2.123$. The J_2/J_1 ratio of 1.79 confirms a diamagnetic $S = 0$ ground state in **Ni5**. At the same time, it becomes evident that the inclusion of the low-temperature magnetization data ($T = 2–5$ K) in Fit III is important to adequately determine an average axial ZFS parameter D for the nickel(II) ions present in **Ni5**, since the ZFS contribution seems to be apparently overestimated, if solely the magnetic susceptibility data is taken into account (Fit I). The average g factor of 2.123 is consistent with the one obtained in Fit II.

To exemplify the importance of the presence of two different exchange coupling constants for the simulation of the magnetic data, the approach in Fit III was modified by constraining the two coupling constants to be equal ($J_1 = J_2$, denoted as Fit IV, see Table S5 and Figure S8, Supporting Information). The obtained g factor of 2.318 is significantly larger than in all other fits performed for **Ni5** which also holds for the coupling constant ($J_1 = J_2 = –47.9\ cm^{-1}$). Moreover, also the obtained average axial ZFS parameter D of $29.6\ cm^{-1}$ is significantly larger than the one obtained in Fit III. Most importantly, this simulation approach (Fit IV) leads to large deviations in the low temperature magnetization and susceptibility data (see Figure S8).

In summary, it can be concluded that for the simulation of the experimental magnetic data of **Ni5**, it is essential to include both a ZFS as well as two different exchange coupling constants according to the spin topology given in Scheme 2. However, the determination of the exact contribution from the magnetic anisotropy of the individual magnetic nickel(II) centers (i.e., absolute value and sign) is far beyond any feasible simulation approach of the experimental data. Nevertheless, this can be supported by high-level ab initio multi-reference calculations, as outlined in the following section.

Computational Studies

For the complex cation of **Ni3** and the neutral complex molecule of **Ni5** quantum mechanical studies were performed to address both the exchange interaction between the nickel(II) ions as well as their individual magnetic anisotropy. For details of the computational approach and the model structures employed see Experimental Section.

Magnetic Exchange Interactions

The individual magnetic exchange interactions present within the trinuclear complex cation of **Ni3** as well as the pentanuclear complex molecule in **Ni5** were studied by broken-symmetry DFT (BS-DFT) calculations.

For **Ni3**, two different approaches have been used.[10b,21] The first approach (denoted as $\mathbf{Ni_2Zn}$) is based on a dinuclear nickel(II) model structure derived from the trinuclear cationic complex **Ni3** for which one paramagnetic nickel(II) ion was replaced by a diamagnetic zinc(II) ion (see Figure S9, Supporting Information). The second approach (denoted as $\mathbf{Ni_3}$) is based on the mapping of the energy difference between the high-spin (HS) and broken-symmetry (BS) state onto pairwise interactions of the nickel(II) ions within the triangular structure. From both approaches $\mathbf{Ni_2Zn}$ and $\mathbf{Ni_3}$, fairly similar values of $–22.0\ cm^{-1}$ and $–23.6\ cm^{-1}$, respectively, for the coupling constant J were obtained (see Table S6, Supporting Information). The corresponding spin density plots for both the HS and BS states resulting from both approaches are depicted Figures S10 and S11 (Supporting Information). Although these values confirm the antiferromagnetic exchange interactions through the N–N diazine bridges of the tritopic triaminoguanidine-based ligand, they somewhat underestimate the experimental value.

To investigate the magnetic exchange interactions in the pentanuclear nickel(II) complex **Ni5**, six different dinuclear nickel(II) model structures were used representing all pairwise spin interactions (**Ni0–Ni1A**, **Ni0–Ni2A**, **Ni0–Ni3B**, **Ni0–Ni4B**, **Ni1A–Ni2A**, and **Ni3B–Ni4B**). For each model structure, the nickel(II) ions not involved in the relevant exchange interaction were replaced by diamagnetic zinc(II) ions (for structures see Figure S12, Supporting Information). The obtained results are summarized in Table S7 (Supporting Information) and clearly verify the presence of antiferromagnetic exchange for all six individual magnetic pair interactions present in the complex molecule of **Ni5**. The corresponding spin-density plots for the HS and BS states of all six dinuclear nickel(II) structural models are depicted in Figures S13 to S18 (Supporting Information).

The weakest antiferromagnetic exchange of $J = –11.8\ cm^{-1}$ is found between the nickel(II) centers Ni0 and Ni3B (**Ni0–Ni3B**). It is interesting to note that for this pair the observed Ni–N–N–Ni dihedral angle of 144.8° shows the largest deviation from the ideal 180° arrangement. At the same time, for

this pair of interacting nickel(II) ions, the greatest deviation from the coplanarity between the π-planes of the central $C(NN)_3$ core of the triaminoguanidine ligand and the phenolate moiety attached to the relevant diazine bridge is observed (40.7°, vide supra). On the other hand, the strongest antiferromagnetic interaction (J = –31.4 cm^{-1}) calculated for the Ni0 and Ni4B pair (**Ni0–Ni4B**) is associated with a dihedral angle for the Ni–N–N–Ni diazine bridge of 170.7° and a deviation from the coplanarity of relevant π-planes of 19.4°. The remaining four pairwise interactions in **Ni5** are found to be in the range from –26.1 to –30.8 cm^{-1}. Overall, there appears to be a trend that increases the antiferromagnetic coupling for these pairwise interactions as the Ni–N–N–Ni dihedral angle increases and the deviation from coplanarity between the relevant π-planes (triaminoguanidine core and phenolate moiety) decreases (cf. Table S7, Supporting Information).

To compare these results with the values obtained from the simulation of the experimental data, the average of the relevant calculated coupling constants must be determined (Γ_1: **Ni0–Ni1A**, **Ni0–Ni2A**, **Ni0–Ni3B**, **Ni0–Ni4B**; Γ_2: **Ni1A–Ni2A**, **Ni3B–Ni4B**). In fact, the average calculated exchange coupling constants Γ_1 = –25.0 cm^{-1} and Γ_2 = –28.6 cm^{-1} are in agreement with the experimental trend ($1 < J_2/J_1 < 2$; J_1 = –20.8 cm^{-1}, J_2 = –37.3 cm^{-1}) and confirm a diamagnetic ground state (S = 0).

Single-Ion Magnetic Anisotropy

To gain insight into the magnetic anisotropy of the paramagnetic centers and to supplement the experimental data of **Ni3** and **Ni5**, ab initio multi-reference calculations have been performed for all crystallographically independent nickel(II) ions of both structures. These studies are based on structurally simplified models in which, with the exception of the nickel(II) ion of interest, all others were replaced by diamagnetic zinc(II) ions. To keep computational cost at an affordable level, further reduction of the system complexity was achieved by replacing the tptz co-ligands attached to the diamagnetic zinc(II) ions with ammonia (NH_3) ligands. The resulting structural models for **Ni3** (denoted as **Ni**) and **Ni5** (denoted as **Ni0**, **Ni1A**, **Ni2A**, **Ni3B**, and **Ni4B**) are depicted in Figures S19 and S20, respectively (Supporting Information). The calculations have been performed in a two-step process, starting with the CASSCF calculations, followed by the inclusion of spin-orbit coupling interactions by CASSCF/RASSI-SO calculations, which allow for the mixing of states of different multiplicities.

CASSCF calculations confirm a high-spin $^3A_{2g}[^3F]$ electronic ground state for all nickel(II) ions in **Ni3** and **Ni5** (see Table S8, Supporting Information). This ground state represents the individual single-ion case, since the employed model structures cannot in principle address additional magnetic exchange. For all nickel(II) centers, the strong distortion of the pseudo-octahedral coordination spheres leads to a significant splitting of the excited high-spin multiplets $^3T_{2g}[^3F]$, $^3T_{1g}[^3F]$, and $^3T_{1g}[^3P]$. The lowest excited single-ion low-spin state is found for the model structure **Ni** (16664 cm^{-1}), which is consistent with the largest distortion from an ideal octahedral coordination geometry observed in **Ni3** [$S(O_h)$ = 2.7]. This is caused by the notable elongation of the Ni–N bonds (Ni–N3: 218.6 pm, Ni–N7: 217.9 pm) of the two axial 2-pyridyl donors of the tptz co-ligand. On the other hand, the highest first excited low-spin state is found for **Ni0** (18301 cm^{-1}), which corresponds to the central nickel(II) center in **Ni5** that shows the least octahedral distortion of all centers due to the absence of a tptz co-ligand. This observed trend is consistent with the hypothetical experiment to continuously elongate the axial Ni–N bonds related to the tptz co-ligand, which would ultimately lead to a low-spin single-ion ground state, as it is known for nickel(II) ions in a square-planar coordination environment.

CASSCF/RASSI-SO calculations were performed to adequately describe the magnetic anisotropy in the $^3A_{2g}[^3F]$ electronic ground state of the investigated metal centers (see Table S9, Supporting Information). This ground multiplet consists of three low-lying spin-orbit coupled states ($(2S+1)\times(2L+1)$ = 3) which are energetically split by the ZFS interaction. The latter can be parameterized by the axial and rhombic ZFS parameters D and E, respectively.

In case of **Ni3**, the calculations for the model structure **Ni** reveal an easy-plane type of magnetic anisotropy with D = 14.4 cm^{-1} for the nickel(II) center (Table S10, Supporting Information). In addition, a significant rhombic distortion of the magnetic anisotropy is apparent (E = 4.4 cm^{-1}) that leads to a pronounced E/D ratio (0.30). The resulting overall energy range for the three relevant states ($D + E$ = 18.8 cm^{-1}) nicely agrees with the experimentally determined ZFS of 20.4 cm^{-1} for **Ni3**. Despite the good agreement, it has to be noted that such ZFS parameters obtained from calculations can depend to a large extend on even subtle differences in the coordination sphere of the metal center.[22] In any case, this is fundamentally different compared to other trinuclear nickel(II) complexes with a triaminoguanidine core, but bpy as co-ligand, for which an easy-axis type of magnetic anisotropy ($D < 0$) is found for the nickel(II) centers.[10b] The orientation of the main anisotropy axes obtained for a single ion leading to the easy-plane anisotropy in **Ni3** is depicted in Figure 6. This shows that the easy-plane axes lie within the plane of the central tritopic triaminoguanidine ligand. The single-ion magnetic anisotropy in **Ni3** can also be described by the Cartesian components of the g tensor (see Table S11 and Figure S21, Supporting Information). This again indicates the presence of a rather large rhombic distortion ($g_x \neq g_y \neq g_z$).

These observations can be rationalized on the basis of donor charges for the relevant ligands (see Figure S22, Supporting Information) obtained by a DFT-based natural population analysis (NPA).[23] In this respect, the nitrogen donor atom (N4) of the triazine moiety of the tptz co-ligand plays a key role, since it shows the second largest negative charge (–0.400) of all relevant donor atoms, with only the phenolate oxygen donor being more negative (–0.700). As a consequence, in **Ni3** the donor atoms of the $[N_3O]$ plane, which is defined by the tridentate pocket of the triaminoguanidine ligand (O1, N1A, N2) and the nitrogen donor of the triazine moiety (N4), possess the largest negative charges. In combination with the elongated Ni–N bonds observed for the two remaining nitrogen donors,

this explains the easy-plane anisotropy. However, the situation is fundamentally different when the tptz co-ligand is replaced by bpy, as it is the case in the complex cation $[Ni_3(saltag^{Br})(bpy)_3(H_2O)_3]^+$, which shows an easy-axis anisotropy due to (i) a weaker additional nitrogen donor of the bpy co-ligand (donor charge: –0.376, see Figure S22, Supporting Information) in the plane defined by the triaminoguanidine ligand, and (ii) considerably shorter axial bonds (Ni–N: 209.4 pm; Ni–O1W: 208.3 pm).[10b]

Five different model structures had to be considered for **Ni5**, all of which lead to a similar splitting of the $^3A_{2g}[^3F]$ ground multiplet in the range of 11.6 to 19.8 cm^{-1} for the five different ions (see Figure S9, Supporting Information). The energetic splitting of the $^3A_{2g}[^3F]$ ground multiplet can also be expressed in terms of the axial and rhombic ZFS parameters D and E, respectively (see Table S10, Supporting Information). In this regard, a clear distinction can be drawn between the central nickel(II) ion **Ni0** and the terminal ones (**Ni1A**, **Ni2A**, **Ni3B**, and **Ni4B**) based on the obtained E/D ratios (**Ni0**: 0.08, **Ni1A**: 0.30, **Ni2A**: 0.27, **Ni3B**: 0.33, **Ni4B**: 0.31), which originates from the different coordination environment, namely the presence of a tptz co-ligand in case of the terminal ions. As a consequence, only the central ion **Ni0** exhibits a distinct easy-axis anisotropy ($D < 0$, $E \approx 0$), whereas the four terminal ions show a large rhombic distortion being close to the maximum ratio of E/D = 1/3. This strong rhombic distortion, however, leads to a situation, in which the magnetic anisotropy cannot solely be interpreted by the sign of the axial ZFS parameter D to be either easy-axis ($D < 0$) or easy-plane ($D > 0$) type. In fact, three of the terminal nickel(II) ions in **Ni5** show a negative D (**Ni1A**: –13.9, **Ni2A**: –13.5, **Ni3B**: –14.9 cm^{-1}), whereas one center is found to exhibit a positive D (**Ni4B**: 14.4 cm^{-1}).

However, the absolute values $|D|$ and $|E|$ are very similar ($|D|$: 13.5–14.9 cm^{-1}; $|E|$ 3.6–4.9 cm^{-1}), which is based on the structural similarity of their coordination environments (see Tables S2 and S3, Supporting Information). In the fit of the experimental data of **Ni5**, an average axial ZFS parameter D of 16.6 cm^{-1} was determined. This D value describes the average energetic splitting of the $^3A_{2g}[^3F]$ ground multiplet for all five nickel(II) ions. Interestingly, by calculating an average $^3A_{2g}[^3F]$ ground state splitting based on the theoretical values given in Table S9 (Supporting Information), a very similar value of 17.1 cm^{-1} can be obtained. The orientation of the anisotropy axes for all five nickel(II) centers is visualized in Figure S23 (Supporting Information). This again can be associated with the donor atom charges of the ligands and the relevant bond lengths. For example, in the case of the nickel(II) centers **Ni1A**, **Ni2A**, and **Ni3B** the orientation of the easy axis is determined by the Ni–N bond of the triazine nitrogen donor (N1i, i = 1,2,3), which are the overall shortest bonds for these centers (Table S3). In addition, the single-ion magnetic anisotropy of the five nickel(II) ions in **Ni5** can be described by the Cartesian components of the g tensor (see Table S11 and Figure S24, Supporting Information). This also reflects the large rhombic anisotropy for **Ni1A**, **Ni2A**, **Ni3B**, and **Ni4B** ($g_x \neq g_y \neq g_z$) as well as the smaller one for **Ni0** ($g_x \approx g_y < g_z$).

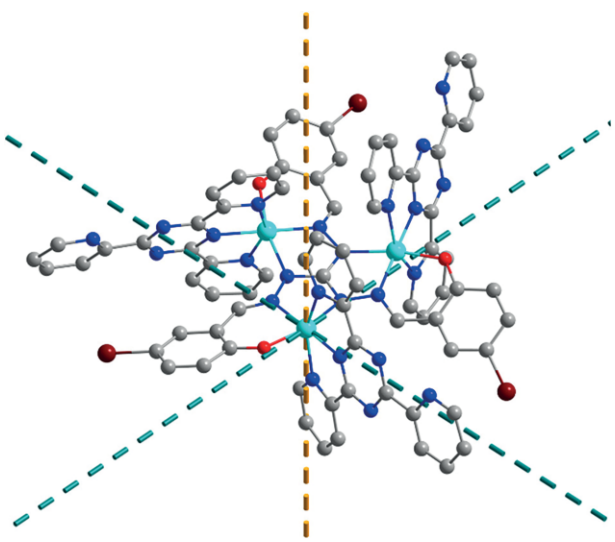

Figure 6. Anisotropy axes (teal dashed lines: easy-plane; orange dashed line: hard-axis) obtained from single-ion ab initio calculations for the $^3A_{2g}[^3F]$ ground state projected on the cationic complex molecule of **Ni3**. Hydrogen atoms are omitted for clarity.

Conclusions

Based on the variation in synthesis it was possible to generate two new nickel(II) complexes of different nuclearity (**Ni3** and **Ni5**) with a tritopic triaminoguanidine derivative as bridging ligand utilizing 2,4,6-tris(2-pyridyl)-1,3,5-triazine (tptz) as additional symmetric co-ligand. The symmetric tridentate binding pocket of the tptz co-ligand together with its planar rigidity leads to a pronounced distortion of the pseudo-octahedral coordination geometry at the individual nickel(II) centers of the trinuclear and pentanuclear complexes **Ni3** and **Ni5**, respectively. Compared to similar complexes with 2,2′-bipyridine (bpy) as co-ligand,[10] this results in distinct differences of their magnetic properties which is mainly due to changes in their magnetic anisotropy. In fact, the exchange coupling constant of **Ni3** is only slightly affected with respect to its bpy analogs due the exchange pathway via the N–N diazine bridges of the triaminoguanidine core which is unaltered and known to be insensitive to variation of its substitution pattern. From the experimental susceptibility and magnetization data it is obvious that an axial ZFS parameter is essential to simulate the magnetic properties, however, with a significantly larger anisotropy observed in the case of the trinuclear (**Ni3** D = 20.4 cm^{-1}) compared to the pentanuclear complex (**Ni5**: D = 16.6 cm^{-1}). For **Ni5**, the ZFS paired with the spin topology given by the "butterfly" motif generated by the two corner-shared triangular units leads to a challenging and fascinating magnetochemistry, since this combination can result in different spin ground states, depending on the actual magnetic exchange between and anisotropy of individual nickel(II) ions. With the help of BS-DFT and ab initio multi-reference CASSCF calculations it was possible to assist the evaluation and assignment of individual magnetic exchange and ZFS parameters, respectively. This has led to the observation of structural correlations with respect to some salient features associ-

ated with the triaminoguanidine bridging core and the co-ligand present. It was found that the sensitive balance between donor strength of the additional donor atom of the co-ligand in the plane defined by the tridentate binding pocket of the triaminoguanidine ligand together with the overall bond length determines the actual character of the magnetic anisotropy at the nickel(II) ions, i.e., easy-axis or easy-plane type. In the case of the magnetic exchange interactions between the nickel(II) centers a twofold dependence on structural features was observed, which is associated with the dihedral angel of the relevant N–N diazine bridge of the triaminoguanidine core and the coplanarity between the relevant π-planes (triaminoguanidine core and phenolate moiety). Besides the tuning of magnetic properties by co-ligand exchange as presented in this work, the design and characterization of corresponding heterometallic complexes is of great interest for future investigations.

Experimental Section

Materials and Physical Measurements: 1,2,3-Tris[(5-bromosalicylidene)amino]guanidine ($H_5saltag^{Br}$) was prepared and subsequently isolated as monohydrochloride salt $H_5saltag^{Br}$·HCl according to literature.[10a,16] All other chemicals and solvents are commercially available and were used as received without further purification. IR spectra of the pure samples were measured on a Bruker IFS55/Equinox spectrometer with a Specac Golden Gate ATR unit. For the measurements of the elemental analyses (C, H, N) a Leco CHNS-932 elemental analyzer was used.

Synthesis of $[Ni_3(saltag^{Br})(tptz)_3]NO_3·4H_2O·6.75CH_3OH$ (Ni3): To a methanol solution (15 mL) of $H_5saltag^{Br}$·HCl (62 mg, 0.089 mmol) was added a mixture of an aqueous solution of $Ni(NO_3)_2·6H_2O$ (73 mg, 0.25 mmol) and a methanol solution (5 mL) of 2,4,6-tris(2-pyridyl)-1,3,5-triazine (78 mg, 0.25 mmol), followed by addition of tetra-*n*-butylammonium hydroxide (0.30 mL, 40 % aqueous solution). The resulting solution was stirred for around 5 min, while a precipitate was formed, which was redissolved by the addition of dmf (5 mL) and the reaction was continued for another 15 min. The resulting solution was filtered and allowed to stand at room temperature. Crystals suitable for X-ray measurement grew within 2 d. Yield: 58 mg (55 %). **IR** (ATR): $\tilde{\nu}$ = 3420 (br., solvent), 1653 (s, –CH=N), 1468, 1441 (triazine –CH=N), 1384 (s, NO_3^-) cm^{-1}. $[Ni_3(saltag^{Br})(tptz)_3]NO_3·4H_2O·6.75CH_3OH$ ($C_{82}H_{67.5}N_{25.5}O_{15.75}Br_3Ni_3$, M = 2077.9 g·mol^{-1}): calcd: C: 47.40, H: 3.27, N: 17.19 %; found: C: 47.41, H: 3.46, N: 17.53 %.

Synthesis of $[Ni_5(saltag^{Br})_2(tptz)_4]·7H_2O·3CH_3OH$ (Ni5): To a dimethylformamide (dmf) solution (15 mL) of $H_5saltag^{Br}$·HCl (62 mg, 0.089 mmol) was added an aqueous (1.5 mL) solution of $Ni(NO_3)_2·6H_2O$ (73 mg, 0.25 mmol), followed by addition of triethylamine (102 mg) dissolved in methanol (3 mL) and the resulting solution was stirred for 15 min, while a precipitate was formed. A methanol (5 mL) solution of 2,4,6-tris(2-pyridyl)-1,3,5-triazine (78 mg, 0.25 mmol) was added stepwise. This caused the dissolution of the mixture and the reaction was continued for 15 min at room temperature. The resulting solution was filtered and allowed to stand at room temperature in a sealed flask. Crystals suitable for X-ray measurement grew after 2 d. Yield: 88 mg (0.04 mmol, 52 %). **IR** (ATR): $\tilde{\nu}$ = 3434 (br., solvent), 1666 (s, –CH=N), 1468, 1433 (triazine –CH=N) cm^{-1}. $[Ni_5(saltag^{Br})_2(tptz)_4]·7H_2O·3CH_3OH$ ($C_{119}H_{98}N_{36}Br_6O_{16}Ni_5$, M = 3061.2 g·mol^{-1}): calcd: C: 46.69, H: 3.23, N: 16.47 %; found: C: 46.53, H: 3.09, N: 16.60 %.

X-ray Crystallography: Crystals of the complex **Ni3** and **Ni5** suitable for X-ray crystallography were obtained directly from the mother liquor. The intensity data were collected at 183 K on a Nonius Kappa CCD diffractometer, using graphite-monochromated Mo-K_α radiation. Data were corrected for Lorentz and polarization effects; absorption was taken into account on a semi-empirical basis using multiple-scans.[24] The structures were solved by direct methods (SHELXS[25]) and refined by full-matrix least-squares techniques against Fo^2 (SHELXL-2018[25]). All hydrogen atoms were included at calculated positions with fixed thermal parameters. The crystals of **Ni3** and **Ni5** contain large voids, filled with disordered solvent molecules. The sizes of the voids are 6215 and 1918 Å^3 per unit cell, respectively. Their contribution to the structure factors was secured by back-Fourier transformation using the SQUEEZE routine of the program PLATON[18] resulting in 1934 and 609 electrons per unit cell, respectively. All non-hydrogen atoms were anisotropically refined.[25]

Crystallographic data (excluding structure factors) for the structures in this paper have been deposited (cf. Tables S12 and S13, Supporting Information) with the Cambridge Crystallographic Data Centre, CCDC, 12 Union Road, Cambridge CB21EZ, UK. Copies of the data can be obtained free of charge on quoting the depository numbers CCDC-2001568 for **Ni3** and CCDC-1969490 for **Ni5** (Fax: +44-1223-336-033; E-Mail: deposit@ccdc.cam.ac.uk, http://www.ccdc.cam.ac.uk)

Magnetic Measurements: Magnetic susceptibility data for **Ni3** and **Ni5** were obtained from powdered samples in gelatin capsules in the temperature range from 2 to 300 K under a dc magnetic field of 2000 Oe using a Quantum-Design MPMS-5 SQUID magnetometer equipped with a 5 T magnet. The measured data were corrected for diamagnetism of the capsule and the intrinsic diamagnetism of the sample, estimated by measurements on a similar ligand system. The molar magnetic susceptibility data of the complexes is based on the molecular weights calculated from the elemental analyses data. Magnetization measurements were performed in the temperature range of 2–5 K in steps of 0.5 K and at magnetic fields from 0 to 5 T. Fitting of the dc SQUID data was performed using the PHI program[19] in version 3.1.5 and the spin Hamiltonians as given in the Equations (1) and (2) for **Ni3** and **Ni5**, respectively.

Computational Details: Structural models for the computational studies are based on the atomic positions of the single-crystal data of **Ni3** and **Ni5**. The position of the hydrogen atoms in these models were optimized at RI-DFT-D3[26]/BP86[27]/def2-SVP[28] level of theory with the program package Turbomole[29] in version 7.2. Within these optimizations all the nickel(II) ions have been replaced by diamagnetic zinc(II) ions to lower the computational effort. Broken-symmetry density functional theory (BS-DFT) calculations were performed utilizing the triple-ζ def2-TZVPP basis sets in combination with the B3-LYP hybrid functional.

For the evaluation of the magnetic coupling constants it was assumed that the energy of the BS state without a spin-projection represents the correct low-spin energy.[30] In the case of **Ni3**, BS-DFT were based on two structural models (see Figure S9, Supporting Information): (i) a cationic trinuclear nickel(II) complex $[Ni_3(saltag^{Br})(tptz)_3]^+$ denoted as **Ni_3** ($\Delta E = E_{BS} - E_{HS} = 6J$), and (ii) a cationic complex $[Ni_2Zn(saltag^{Br})(tptz)_3]^+$ denoted as **Ni_2Zn**, in which one nickel(II) center was replaced by diamagnetic zinc(II) ion ($\Delta E = E_{BS} - E_{HS} = 3J$). For the pentanuclear nickel(II) complex **Ni5**, six model structures of the composition $[Ni_2Zn_3(saltag^{Br})_2(tptz)_4]$ were used (see Figure S12, Supporting Information), namely **Ni0–Ni1A**, **Ni0–Ni2A**, **Ni0–Ni3B**, **Ni0–Ni4B**, **Ni1A–Ni2A**, and **Ni3B–Ni4B**, for which the

nickel(II) ions not of interest were replaced by diamagnetic zinc(II) ions ($\Delta E = E_{BS} - E_{HS} = 3J$).

Single-ion CASSCF/RASSI-SO ab initio calculations for model structures of all crystallographically independent nickel(II) ions in **Ni3** and **Ni5** were performed with the OpenMOLCAS package of programs in version 18.09.[31] For all model structures all nickel(II) ions, except the one of interest, were replaced by diamagnetic zinc(II) ions to keep the computational effort feasible. To further reduce the computational cost all tptz co-ligands not attached to the relevant nickel(II) centers were replaced by ammonia (NH_3) ligands. For the cationic trinuclear nickel(II) complex for **Ni3** this leads to the model structure depicted in Figure S19 (Supporting Information) (denoted as **Ni**), whereas the five model structures obtained for **Ni5** are depicted in Figure S20 (Supporting Information) (denoted as **Ni0**, **Ni1A**, **Ni2A**, **Ni3B**, **Ni4B**). State-averaged CASSCF calculations with 8 electrons in 10 orbitals (3d and 4d shell) were performed for 10 high-spin ($S = 1$) and 15 low-spin ($S = 0$) states for all model structures. A scalar-relativistic Douglas–Kroll–Hess Hamiltonian of the second order in combination with ANO-RCC basis sets for all atoms was employed to adequately take relativistic effects into account (see Table S14, Supporting Information, for basis set details).[32] Subsequently, spin–orbit coupling interactions, which allow a mixing of states of different multiplicities, were included by the RASSI-SO program. The SINGLE_ANISO module was used to obtain magnetic properties such as *g* factors and zero-field splitting (ZFS) parameters for the nickel(II) centers.

Supporting Information (see footnote on the first page of this article): Structural details including bond lengths and representations of coordination polyhedra, details on the magnetic characterization, DFT ligand studies, BS-DFT computational models and results, ab initio computational models and results.

Acknowledgements

We thank *Dr. Daniel Plaul* for his support in the design of the synthetic procedures. We also want to emphasize our appreciation for the persistence of one of the reviewers of this manuscript. Open access funding enabled and organized by Projekt DEAL.

Keywords: Nickel; Triaminoguanidine; Quantum chemistry; Magnetochemistry; Magnetic anisotropy

References

[1] a) R. H. Holm, P. Kennepohl, E. I. Solomon, *Chem. Rev.* **1996**, *96*, 2239–2314; b) D. Buccella, M. H. Lim, J. R. Morrow, *Inorg. Chem.* **2019**, *58*, 13505–13508.
[2] a) M. G. White, *Catal. Today* **1993**, *18*, 73–109; b) D. S. Nesterov, O. V. Nesterova, A. J. L. Pombeiro, *Coord. Chem. Rev.* **2018**, *355*, 199–222; c) N. Manicke, S. Hoof, M. Keck, B. Braun-Cula, M. Feist, C. Limberg, *Inorg. Chem.* **2017**, *56*, 8554–8561.
[3] a) J. M. Frost, K. L. M. Harriman, M. Murugesu, *Chem. Sci.* **2016**, *7*, 2470–2491; b) G. E. Kostakis, S. P. Perlepes, V. A. Blatov, D. M. Proserpio, A. K. Powell, *Coord. Chem. Rev.* **2012**, *256*, 1246–1278; c) J. B. Peng, Q. C. Zhang, X. J. Kong, Y. Z. Zheng, Y. P. Ren, L. S. Long, R. B. Huang, L. S. Zheng, Z. Zheng, *J. Am. Chem. Soc.* **2012**, *134*, 3314–3317; d) I. Doroshenko, M. Babiak, A. Buchholz, J. Tucek, W. Plass, J. Pinkas, *New J. Chem.* **2018**, *42*, 1931–1938; e) I. Doroshenko, M. Babiak, A. Buchholz, H. Görls, W. Plass, J. Pinkas, *New J. Chem.* **2018**, *42*, 9568–9577.
[4] a) D. Maniaki, E. Pilichos, S. P. Perlepes, *Front. Chem.* **2018**, *6*, 461; b) K. S. Pedersen, J. Bendix, R. Clerac, *Chem. Commun.* **2014**, *50*, 4396–4415; c) D. Gatteschi, R. Sessoli, J. Villain, *Molecular Nanomagnets*, Oxford University Press, Oxford, **2006**; d) *Magnetism: Molecules to Materials, Vol. I–V* (Eds.: J. S. Miller, M. Drillon), Wiley-VCH, Weinheim, **2001–2005**; e) W. Plass, *Chem. Unserer Zeit* **1998**, *32*, 323–333.
[5] a) T. Shiga, G. N. Newton, H. Oshio, *Dalton Trans.* **2018**, *47*, 7384–7394; b) S.-L. Huang, T. S. A. Hor, G.-X. Jin, *Coord. Chem. Rev.* **2017**, *333*, 1–26; c) Y.-Y. Zhang, W.-X. Gao, L. Lin, G.-X. Jin, *Coord. Chem. Rev.* **2017**, *344*, 323–344; d) H. Li, Z.-J. Yao, D. Liu, G.-X. Jin, *Coord. Chem. Rev.* **2015**, *293–294*, 139–157.
[6] C. von Eßen, C. R. Göb, I. M. Oppel, *Triaminoguanidinium-Based Ligands in Supramolecular Chemistry*, in *Guanidines as Reagents and Catalysts II* (Ed.: P. Selig), Springer International Publishing, Cham, **2017**, pp. 75–94.
[7] a) I. M. Müller, R. Robson, *Angew. Chem. Int. Ed.* **2000**, *39*, 4357–4359; b) I. M. Müller, R. Robson, F. Separovic, *Angew. Chem. Int. Ed.* **2001**, *40*, 4385–4386; c) I. M. Müller, S. Spillmann, H. Franck, R. Pietschnig, *Chem. Eur. J.* **2004**, *10*, 2207–2213; d) I. M. Müller, D. Möller, K. Föcker, *Chem. Eur. J.* **2005**, *11*, 3318–3324; e) I. M. Oppel, K. Föcker, *Angew. Chem. Int. Ed.* **2008**, *47*, 402–405.
[8] W. Plass, *Coord. Chem. Rev.* **2009**, *253*, 2286–2295.
[9] a) A. Zharkouskaya, A. Buchholz, W. Plass, *Eur. J. Inorg. Chem.* **2005**, 4875–4879; b) A. Zharkouskaya, H. Görls, G. Vaughan, W. Plass, *Inorg. Chem. Commun.* **2005**, *8*, 1145–1148.
[10] a) A. E. Ion, E. T. Spielberg, H. Görls, W. Plass, *Inorg. Chim. Acta* **2007**, *360*, 3925–3931; b) M. Böhme, D. Schuch, A. Buchholz, H. Görls, W. Plass, *Z. Anorg. Allg. Chem.* **2020**, doi: 10.1002/zaac.201900288.
[11] D. Plaul, M. Böhme, S. Ostrovsky, Z. Tomkowicz, H. Görls, W. Haase, W. Plass, *Inorg. Chem.* **2018**, *57*, 106–119.
[12] a) B. Kintzel, M. Böhme, J. Liu, A. Burkhardt, J. Mrozek, A. Buchholz, A. Ardavan, W. Plass, *Chem. Commun.* **2018**, *54*, 12934–12937; b) E. T. Spielberg, A. Gilb, D. Plaul, D. Geibig, D. Hornig, D. Schuch, A. Buchholz, A. Ardavan, W. Plass, *Inorg. Chem.* **2015**, *54*, 3432–3438.
[13] J. Liu, J. Mrozek, W. K. Myers, G. A. Timco, R. E. P. Winpenny, B. Kintzel, W. Plass, A. Ardavan, *Phys. Rev. Lett.* **2019**, *122*, 037202.
[14] a) A. J. Finney, M. A. Hitchman, C. L. Raston, G. L. Rowbottom, A. H. White, *Aust. J. Chem.* **1981**, *34*, 2139–2157; b) H. Adams, S. Clunas, D. E. Fenton, D. N. Towers, *J. Chem. Soc., Dalton Trans.* **2002**, 3933–3935; c) K. Darling, W. Ouellette, A. Prosvirin, S. Walter, K. R. Dunbar, J. Zubieta, *Polyhedron* **2013**, *58*, 18–29.
[15] a) S. Das, L. Sorace, A. Guha, R. Sanyal, H. Kara, A. Caneschi, E. Zangrando, D. Das, *Eur. J. Inorg. Chem.* **2014**, *2014*, 2753–2765; b) A. Escuer, J. Esteban, J. Mayans, M. Font-Bardia, *Eur. J. Inorg. Chem.* **2014**, *2014*, 5443–5450; c) Y.-W. Tzeng, C.-J. Lin, M. Nakano, C.-I. Yang, W.-L. Wan, L.-L. Lai, *Dalton Trans.* **2014**, *43*, 3044–3047.
[16] I. M. Müller, D. Möller, *Eur. J. Inorg. Chem.* **2005**, 257–263.
[17] G. Socrates, *Infrared and Raman characteristic group frequencies: Tables and charts*, third ed., John Wiley & Sons, **2004**.
[18] A. L. Spek, *Acta Crystallogr., Sect C* **2015**, *71*, 9–18 .
[19] N. F. Chilton, R. P. Anderson, L. D. Turner, A. Soncini, K. S. Murray, *J. Comput. Chem.* **2013**, *34*, 1164–1175.
[20] a) W. Plass, *Inorg. Chem.* **1997**, *36*, 2200–2205; b) O. Kahn, *Molecular Magnetism*, VCH-Wiley, Weinheim, **1993**.
[21] a) E. T. Spielberg, M. Fittipaldi, D. Geibig, D. Gatteschi, W. Plass, *Inorg. Chim. Acta* **2010**, *363*, 4269–4276; b) D. Plaul, D. Geibig, H. Görls, W. Plass, *Polyhedron* **2009**, *28*, 1982–1990.
[22] a) M. Rams, M. Böhme, V. Kataev, Y. Krupskaya, B. Büchner, W. Plass, T. Neumann, Z. Tomkowicz, C. Näther, *Phys. Chem. Chem. Phys.* **2017**, *19*, 24534–24544; b) M. Rams, Z. Tomkowicz, M. Böhme, W. Plass, S. Suckert, J. Werner, I. Jess, C. Näther, *Phys. Chem. Chem. Phys.* **2017**, *19*, 3232–3243; c) M. Rams, A.

Jochim, M. Böhme, T. Lohmiller, M. Ceglarska, M. M. Rams, A. Schnegg, W. Plass, C. Näther, *Chem. Eur. J.* **2019**, doi: 10.1002/chem.201903924; d) M. Böhme, A. Jochim, M. Rams, T. Lohmiller, S. Suckert, A. Schnegg, W. Plass, C. Näther, *Inorg. Chem.* **2020**, doi: 10.1021/acs.inorgchem.1029b03357.
[23] A. E. Reed, R. B. Weinstock, F. Weinhold, *J. Chem. Phys.* **1985**, *83*, 735–746.
[24] a) O. Rådmark, B. Samuelsson, *J. Lipid. Res.* **2009**, *50*, S40-S45; b) Z. Otwinowski, W. Minor, *Processing of X-ray diffraction data collected in oscillation mode*, in *Methods in Enzymology, Vol. 276*, Academic Press, **1997**, pp. 307–326; c) L. Krause, R. Herbst-Irmer, G. M. Sheldrick, D. Stalke, *J. Appl. Crystallogr.* **2015**, *48*, 3–10.
[25] G. M. Sheldrick, *Acta Crystallogr. Sect.C* **2015**, *71*, 3–8.
[26] a) E. J. Baerends, D. E. Ellis, P. Ros, *Chem. Phys.* **1973**, *2*, 41–51; b) B. I. Dunlap, J. W. D. Connolly, J. R. Sabin, *J. Chem. Phys.* **1979**, *71*, 3396–3402; c) S. Grimme, J. Antony, S. Ehrlich, H. Krieg, *J. Chem. Phys.* **2010**, *132*, 154104; d) C. Van Alsenoy, *J. Comput. Chem.* **1988**, *9*, 620–626; e) J. L. Whitten, *J. Chem. Phys.* **1973**, *58*, 4496–4501.
[27] a) A. D. Becke, *Phys. Rev. A* **1988**, *38*, 3098–3100; b) J. P. Perdew, *Phys. Rev. B* **1986**, *33*, 8822–8824.
[28] F. Weigend, R. Ahlrichs, *Phys. Chem. Chem. Phys.* **2005**, *7*, 3297–3305.
[29] Y. Sugiura, H. Tanaka, Y. Mino, T. Ishida, N. Ota, M. Inoue, K. Nomoto, H. Yoshioka, T. Takemoto, *J. Am. Chem. Soc.* **1981**, *103*, 6979–6982.
[30] a) J. P. Perdew, A. Savin, K. Burke, *Phys. Rev. A* **1995**, *51*, 4531–4541; b) J. P. Perdew, M. Ernzerhof, K. Burke, A. Savin, *Int. J. Quantum Chem.* **1997**, *61*, 197–205; c) E. Ruiz, S. Alvarez, J. Cano, V. Polo, *J. Chem. Phys.* **2005**, *123*, 164110.
[31] I. F. Galván, M. Vacher, A. Alavi, C. Angeli, F. Aquilante, J. Autschbach, J. J. Bao, S. I. Bokarev, N. A. Bogdanov, R. K. Carlson, L. F. Chibotaru, J. Creutzberg, N. Dattani, M. G. Delcey, S. S. Dong, A. Dreuw, L. Freitag, L. M. Frutos, L. Gagliardi, F. Gendron, A. Giussani, L. González, G. Grell, M. Guo, C. E. Hoyer, M. Johansson, S. Keller, S. Knecht, G. Kovačević, E. Källman, G. Li Manni, M. Lundberg, Y. Ma, S. Mai, J. P. Malhado, P. Å. Malmqvist, P. Marquetand, S. A. Mewes, J. Norell, M. Olivucci, M. Oppel, Q. M. Phung, K. Pierloot, F. Plasser, M. Reiher, A. M. Sand, I. Schapiro, P. Sharma, C. J. Stein, L. K. Sørensen, D. G. Truhlar, M. Ugandi, L. Ungur, A. Valentini, S. Vancoillie, V. Veryazov, O. Weser, T. A. Wesołowski, P.-O. Widmark, S. Wouters, A. Zech, J. P. Zobel, R. Lindh, *J. Chem. Theory Comput.* **2019**, *15*, 5925–5964.
[32] a) B. O. Roos, R. Lindh, P.-Å. Malmqvist, V. Veryazov, P.-O. Widmark, *J. Phys. Chem. A* **2004**, *108*, 2851–2858; b) B. O. Roos, R. Lindh, P.-Å. Malmqvist, V. Veryazov, P.-O. Widmark, *J. Phys. Chem. A* **2005**, *109*, 6575–6579; c) P.-O. Widmark, P.-A. Malmqvist, B. O. Roos, *Theor. Chim. Acta* **1990**, *77*, 291–306.

Received: February 5, 2020

